CFSRC COLLOQUIUM

Proceedings of the Cold-Formed Steel Research Consortium Colloquium
20-22 October 2020 (cfsrc.org)

Large Deflection Analysis of Beam-Columns with General Sections Using Gaussian Line-element Method

A.H.A. Abdelrahman[1], Liang Chen[2], Siwei Liu[3], Ronald D. Ziemian[4] and Siu-Lai Chan[5]

Abstract

The line-element analysis method is extensively adopted in practicing engineering, relying on the robustness of the basic beam-column element formulations. This paper proposes a new beam-column element based on the nonsymmetrical section assumption for large deflection analysis of beam-columns with general sections. The element formulations are derived by introducing the total-potential energy method. When the member is under torsion, the inclined angle, between the cross-section's and the element's local axes, is varied along the element length due to the twisting, thereby causing the difficulty in summating the section stiffness to form the element stiffness matrix. To this end, the Gaussian quadrature method is introduced to this summation process. A refined Updated-Lagrangian method (UL) is developed for considering large deflection. The major feature of this element, as compared with others, is the proper consideration of the twisting deformation within the element, allowing the use of fewer elements to simulate a structural member for dramatically increasing the numerical efficiency. Detailed derivations are given, and their implementations are elaborated. Finally, several validation examples are provided for verifying the accuracy and examining the robustness of the proposed method.

1. Introduction

Thin-walled asymmetrical section members are extensively used in contemporary structures for improving material usage efficiency. Further, the high strength-to-weight and stiffness-to-weight ratios make such members show superiority for cold-formed and modular steel constructions. The constraints of fabricating irregularly shaped sections, such as those in Figure 1, are eliminated as robotic welding machines (RWM), and building information modelling (BIM) are extensively utilized in modern steel constructions. However, the large-deflection behavior of these members is usually complex, thereby eliminating the use of the direct analysis method (DAM) for structures of which members with asymmetrical sections are a part.

Direct analysis method (DAM), also named as a second-order design approach, is considered an innovative and robust method at which the real behavior of the structures is included within the analysis. Current design specifications such as AISC360-16 (2016) and Eurocode-3 (2005) highly recommend DAM as a primary method to design structures for stability. Accordingly, the evolution of member checking moves from system level (K factors) to a member physical length (buckling curve) and right down to the cross-section level (section capacity check). With this purpose, different numerical methods, such as the shell finite-element method (SFEM) (Abdelrahman et al. 2019; Abdelrahman et al. 2020; G. Bian 2017; Hussain et al. 2018; Schafer & Peköz 1998; Tang et al. 2018; Yu & Schafer 2007), generalized beam theory (GPT) (Dinis et al. 2006; Gonçalves et al. 2010; Martins et al. 2018a; Martins et al. 2018b), finite-strip method (FSM) (Ádány & Schafer 2014; Guanbo Bian et al. 2016; Schafer 2002), and line finite-element method (LFEM) (Chan & Cho 2008; Cho & Chan 2008; Du et al. 2017; Hancock & Rasmussen 2016; Shakourzadeh et al. 1995), are provided for investigating the buckling behaviour of asymmetrical section members thereby conducting an advanced analysis of structures comprising such members.

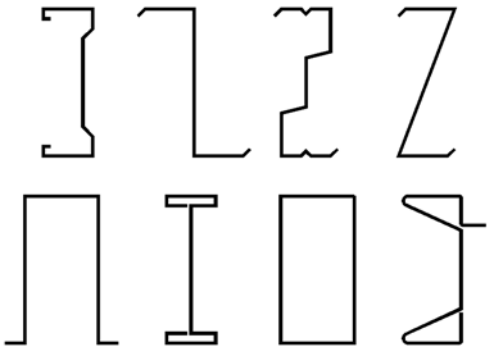

Figure 1. Examples of irregularly-shaped sections in cold-formed and modular constructions

[1]*Lecturer, Department of Structural Engineering, Mansoura University, Egypt.*
[2]*Ph.D Candidate, Civil and Environmental Engineering, The Hong Kong Polytechnic University, Hong Kong, China.*
[3]*Associate Professor, School of Civil Engineering, Sun Yat-Sen University, China.*
[4]*Professor, Civil Engineering, Bucknell University, USA.*
[5]*Chair Professor, Civil and Environmental Engineering, The Hong Kong Polytechnic University, Hong Kong, China.*

Line finite-element method (LFEM) is extensively employed in current engineering practices to simulate the global behavior of members and systems, as it is considered the most efficient over the other numerical methods. Such a method shows superiority in terms of computational efficiency and convenience in programming. However, the accuracy of LFEM mainly relies on the robustness of the element formulation as well as the deep consideration of the actual member and system deformations, thereby underpinning the development of the direct analysis method. As such a requirement, several advanced line-elements are derived, such as Hermite cubic element (Bathe et al. 1979; Chan & Zhou 1994; Connor et al. 1968; Fong & Chan 2012; Iu & Bradford 2010; Teh 2001; Wood & Zienkiewicz 1977), stability function element (Chan & Gu 2000; W. F. Chen & Lui 1987; Liew et al. 1999; Oran 1973), force-based line element (Du et al. 2017; Neuenhofer & Filippou 1997, 1998; Souza 2000; Spacone et al. 1996), mixed field element (K. J. Bathe 2007; Zienkiewicz et al. 2005), high-order shape function element (Bai et al. 2020; Bai et al. 2019; Izzuddin & Smith 1996; Liu et al. 2014a, 2014b; So & Chan 1991) and warping line element (Chan & Kitipornchai 1987; Hancock & Rasmussen 2016; Kim et al. 1996; Liu et al. 2019; Liu et al. 2018; Shakourzadeh et al. 1995; Ziemian et al. 2019). The main features and the drawbacks of these elements are briefly elaborated, as shown in Figure 2.

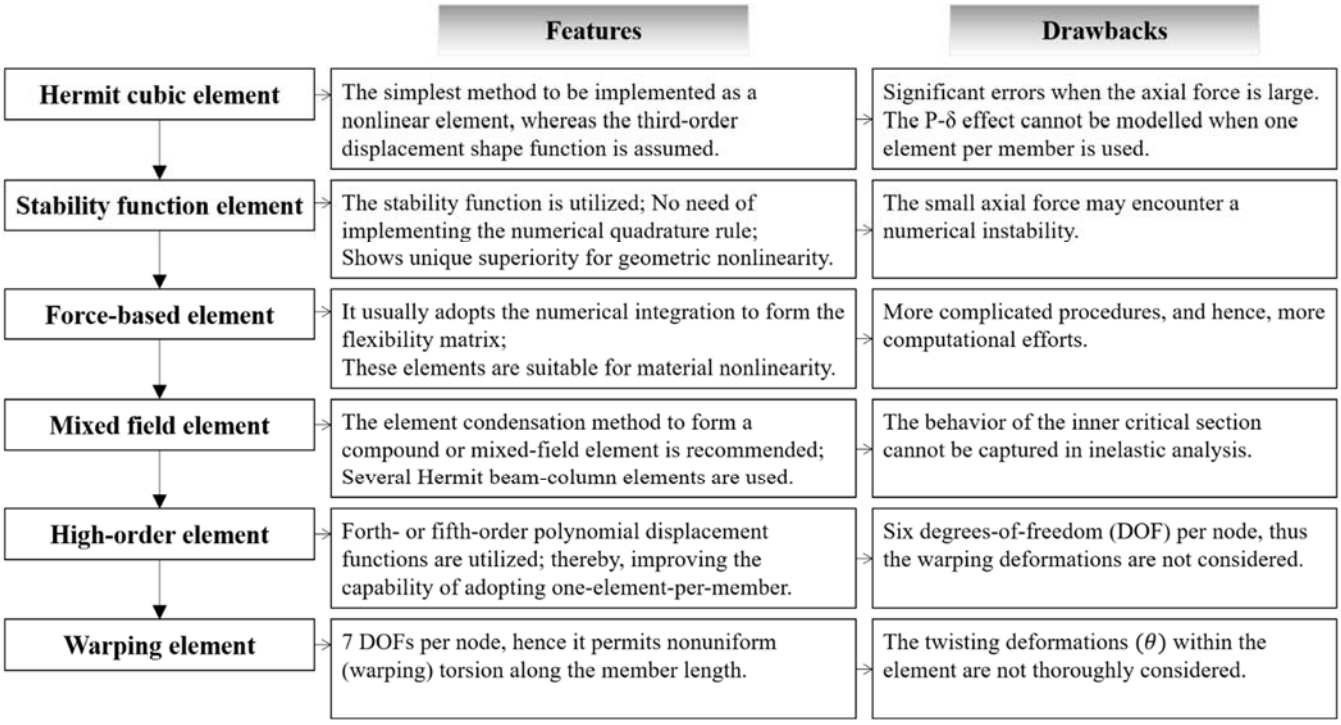

Figure 2. The main features and drawbacks of different line elements

In recent years, more researchers have been devoted to considering Wagner effects in the formulation of the beam-column elements for asymmetrical sections' members (Gao et al. 2020; Liu et al. 2019; Liu et al. 2018). For example, Hancock and Rasmussen (2016) developed an advanced flexibility-based beam-column element with seven degrees of freedom (DOFs) whereas the misalignment of the shear center and the centroid is taken into consideration. Their routine has been programmed into OpenSEES (Mazzoni et al. 2006). Later, Ronald Zimeian and his co-workers developed a displacement-based line element with warping degree of freedom, which implement the Updated-Lagrangian (UL) description for tracking the large-deflection behaviour (Liu et al. 2019; Liu et al. 2018). The derivations and the element formulations were illustrated, while the numerical implementation within the educational software MASTAN2 (Ziemian et al. 2019) was presented. Although recent research has made a significant contribution to simulating such complex behaviors of thin-walled members, there are still improvements that can be made.

Generally, the non-coincidence of the centroid and the shear center of asymmetric section's members makes the global member's behavior apparently different. The member twisting causes the inclination between the member's local axes and the cross-section axes. As a result, the cross-section properties, such as coordinates of the shear center with respect to the centroid (y_s and z_s) as well as the Wagner coefficients (β_y, β_z, and β_ω), are varied along the member length. This demonstrates the need for inclusion of the

twisting angle (θ) without an error of assuming the cross-section being unchangeable. Accordingly, more accurate predictions of the member deformations along the member length are established utilizing fewer elements to model the member (Figure 3). It is believed that the twisting angles along the element need to be considered, thereby predicting the global behavior of asymmetrical section members under high twisting levels.

In this paper, a new Gaussian beam-column (GBC) element is derived, and the detailed formulations are presented. The Gauss-quadrature method is implemented so that the twisting angle along the element length is included in the element's formulations. The numerical procedure is illustrated. Finally, verification examples are provided, and the accuracy of the proposed method is clearly established.

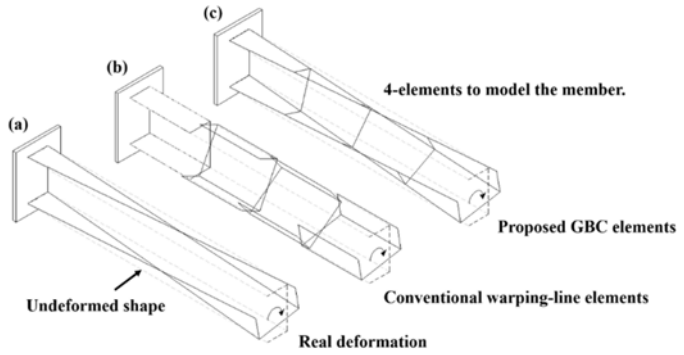

Figure 3. Illustration of the simulations using conventional warping line-element and proposed Gaussian beam-column (G.B.C.) elements

2. Assumption

For the element formulations, the following assumptions are made; (1) the material is elastic, homogenous, and isotropic, (2) strains are small, but the deformations and displacements can be large, (3) the applied loads are conservative, and (4) section local, and distortional buckling are not taken into account.

3. Gauss Line-Element Formulation

In the following, a new gaussian beam-column element is derived so that the twisting angle (θ) along the element length is considered in the element derivation. Thus, the element formulations and its implementation for large deflection analysis of thin-walled members are presented. As a sequel, element's local axes and forces, the total potential energy function, Gaussian quadrature method, section properties at each gaussian point, and the tangent stiffness matrix are provided in detail.

3.1 Element Local Axes and Forces

Because asymmetrical section members usually experience apparent warping deformations, an additional degree-of-freedom DOF (i.e. warping DOF) is proposed so that a 14 DOFs element is introduced (Figure 4). The element local axes, as well as the element's deformations and forces, are shown in Figure 4. It is worthy of mentioning that the centroidal axis connecting the section centroids at element ends is of a spiral line due to the element twisting along its length (Figure 4). For the derivation, only the longitudinal axial displacement (u) is referenced to the centroidal axis, while the other deformations are defined with respect to the shear-center axis. After the derivations, however, they are transferred to the section centroid utilizing a transformation matrix presented later in this paper.

To describe the deformations along the element length, fourth-order displacement shape functions are implemented. Because the twisting deformations (θ) are essential to be calculated at each gaussian point, the following relation is adopted and given for easy reference as;

$$\theta(x) = \left(x - \frac{2x^2}{L} + \frac{x^3}{L^2}\right)\theta_{b1} + \left(-\frac{x^2}{L} + \frac{x^3}{L^2}\right)\theta_{b2} + \left(1 - \frac{3x^2}{L^2} + \frac{2x^3}{L^3}\right)\theta_{x1} + \left(\frac{3x^2}{L^2} - \frac{2x^3}{L^3}\right)\theta_{x2} \quad (1)$$

where $\theta(x)$ is the twisting angle along the element length; θ_{x1} and θ_{x2} are the twisting angles at the element ends; and θ_{b1} and θ_{b2} are the corresponding warping angles.

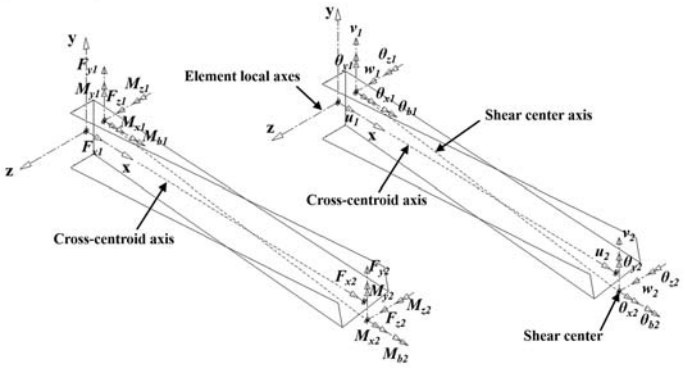

Figure 4. Illustrations of the deformations and forces in the element local axes

3.2 Total Potential Energy

The element stiffness matrix can be derived by the second variation of the total potential energy function, which is given as;

$$\Pi = U - V \quad (2)$$

in which, Π is the total potential energy, V is the work done by external loads, and U is the strain energy which can be calculated by,

$$U \approx \frac{1}{2}\int_0^L \left[EA\left(\frac{\partial u_0(x)}{\partial x}\right)^2 + EI_\omega\left(\frac{\partial^2\theta(x)}{\partial x^2}\right)^2 + GJ\left(\frac{\partial\theta(x)}{\partial x}\right)^2\right]dx + \frac{1}{2}\int_0^L P\left[\left(\frac{\partial v_0(x)}{\partial x}\right)^2 + \left(\frac{\partial w_0(x)}{\partial x}\right)^2\right]dx + \frac{1}{2}\int_0^L Pr^2\left(\frac{\partial\theta(x)}{\partial x}\right)^2 dx + \int_0^L M_{y1}\frac{L-x}{L}\frac{\partial\theta(x)}{\partial x}\frac{\partial v_0(x)}{\partial x}dx - \int_0^L M_{y2}\frac{x}{L}\frac{\partial\theta(x)}{\partial x}\frac{\partial v_0(x)}{\partial x}dx + \int_0^L M_{z1}\frac{L-x}{L}\frac{\partial\theta(x)}{\partial x}\frac{\partial w_0(x)}{\partial x}dx - \int_0^L M_{z2}\frac{x}{L}\frac{\partial\theta(x)}{\partial x}\frac{\partial w_0(x)}{\partial x}dx + \int_0^L \left[\frac{-M_{z1}-M_{z2}}{L}\left(\theta(x)\frac{\partial w_0(x)}{\partial x} - \frac{\partial u_0(x)}{\partial x}\frac{\partial v_0(x)}{\partial x}\right) - \frac{M_{y1}+M_{y2}}{L}\left(\theta(x)\frac{\partial v_0(x)}{\partial x} + \frac{\partial u_0(x)}{\partial x}\frac{\partial w_0(x)}{\partial x}\right)\right]dx + \frac{1}{2}\int_0^L \left[EI_{z\theta}\left(\frac{\partial^2 v_0(x)}{\partial x^2}\right)^2 + EI_{y\theta}\left(\frac{\partial^2 w_0(x)}{\partial x^2}\right)^2\right]dx + \frac{1}{2}\int_0^L M_b\beta_{\omega\theta}\left(\frac{\partial\theta(x)}{\partial x}\right)^2 dx + \frac{1}{2}\int_0^L P\left[2y_{s\theta}\frac{\partial w_0(x)}{\partial x} - 2z_{s\theta}\frac{\partial v_0(x)}{\partial x}\right]\frac{\partial\theta(x)}{\partial x}dx + \int_0^L M_{y1}\frac{L-x}{L}\frac{\partial\theta(x)}{\partial x}\left[\frac{1}{2}\beta_{y\theta}\frac{\partial\theta(x)}{\partial x}\right]dx - \int_0^L M_{y2}\frac{x}{L}\frac{\partial\theta(x)}{\partial x}\left[\frac{1}{2}\beta_{y\theta}\frac{\partial\theta(x)}{\partial x}\right]dx + \int_0^L M_{z1}\frac{L-x}{L}\frac{\partial\theta(x)}{\partial x}\left[\frac{1}{2}\beta_{z\theta}\frac{\partial\theta(x)}{\partial x}\right]dx - \int_0^L M_{z2}\frac{x}{L}\frac{\partial\theta(x)}{\partial x}\left[\frac{1}{2}\beta_{z\theta}\frac{\partial\theta(x)}{\partial x}\right]dx \quad (3)$$

where, $y_{s\theta}$, $z_{s\theta}$, $I_{y\theta}$, $I_{z\theta}$, $\beta_{y\theta}$, $\beta_{z\theta}$, and $\beta_{\omega\theta}$ are section properties calculated at different gaussian points along the element length with respect to the twisting angle (θ) (Figure 5).

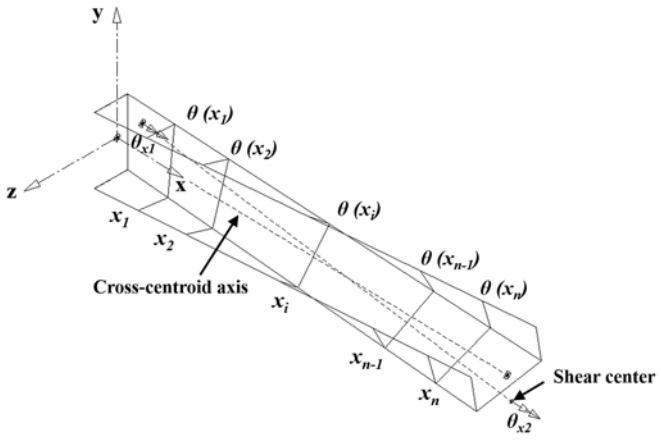

Figure 5. Gaussian points along the element length

3.3 Gauss Integration Method and Section Properties at Each Gaussian Point

When the element twists, the inclination angle (θ) between the cross-section's axes and element's local axes is calculated according to the shape interpolation function (equation (1)), and hence, the cross-section properties, such as the coordinates of the shear center with respect the centroid ($y_{s\theta}$ and $z_{s\theta}$) as well as the second moment of areas ($I_{y\theta}$ and $I_{z\theta}$), are varied along the element length. As a result, the direct integration of equation (3) is mathematically complex; accordingly, the Gaussian quadrature method is introduced to summate the cross-section properties along the element length thereby integrating the potential energy function. With this purpose, a number of 5 gaussian points is placed along the element length, as shown in Figure 5, where the location of each Gaussian point is determined by the Gauss quadrature method and the updated coordinates of the cross-section ($z_{s\theta}$, $y_{s\theta}$) of any point (z, y) after the element twisting can be calculated as follows,

$$y_{\theta i} = y\cos\big(\theta(x_i)\big) + z\sin\big(\theta(x_i)\big) \quad (4)$$

$$z_{\theta i} = z\cos\big(\theta(x_i)\big) - y\sin\big(\theta(x_i)\big) \quad (5)$$

Besides, the section properties at the i^{th} Gaussian point (Figure 6) can be generated by,

$$y_{s\theta i} = y_s\cos\big(\theta(x_i)\big) + z_s\sin\big(\theta(x_i)\big) \quad (6)$$

$$z_{s\theta i} = z_s\cos\big(\theta(x_i)\big) - y_s\sin\big(\theta(x_i)\big) \quad (7)$$

$$I_{y\theta i} = \int_A z_{\theta i}^2\, dA \quad (8)$$

$$I_{z\theta i} = \int_A y_{\theta i}^2\, dA \quad (9)$$

$$\beta_{y\theta i} = \frac{1}{I_{y\theta i}}\int_A (z_{\theta i}^3 + z_{\theta i}y_{\theta i}^2)dA - 2z_{s\theta i} \quad (10)$$

$$\beta_{z\theta i} = \frac{1}{I_{z\theta i}}\int_A (y_{\theta i}^3 + y_{\theta i}z_{\theta i}^2)dA - 2y_{s\theta i} \quad (11)$$

$$\beta_{\omega\theta i} = \frac{1}{I_\omega}\int_A \omega_n\,(y_{\theta i}^2 + z_{\theta i}^2)dA \quad (12)$$

With these in hand, the strain energy sorted in the element is simplified and presented as follows,

$$
\begin{aligned}
&U \\
&\approx \frac{1}{2}\int_0^L \left[EA\left(\frac{\partial u_0(x)}{\partial x}\right)^2 + EI_\omega \left(\frac{\partial^2 \theta(x)}{\partial x^2}\right)^2 \right. \\
&\left. + GJ\left(\frac{\partial \theta(x)}{\partial x}\right)^2 \right] dx \\
&+ \frac{1}{2}\int_0^L P\left[\left(\frac{\partial v_0(x)}{\partial x}\right)^2 + \left(\frac{\partial w_0(x)}{\partial x}\right)^2\right] dx \\
&+ \frac{1}{2}\int_0^L Pr^2\left(\frac{\partial \theta(x)}{\partial x}\right)^2 dx \\
&+ \int_0^L M_{y1}\frac{L-x}{L}\frac{\partial \theta(x)}{\partial x}\frac{\partial v_0(x)}{\partial x} dx \\
&- \int_0^L M_{y2}\frac{x}{L}\frac{\partial \theta(x)}{\partial x}\frac{\partial v_0(x)}{\partial x} dx \\
&+ \int_0^L M_{z1}\frac{L-x}{L}\frac{\partial \theta(x)}{\partial x}\frac{\partial w_0(x)}{\partial x} dx \\
&- \int_0^L M_{z2}\frac{x}{L}\frac{\partial \theta(x)}{\partial x}\frac{\partial w_0(x)}{\partial x} dx \\
&+ \int_0^L \left[\frac{-M_{z1}-M_{z2}}{L}\left(\theta(x)\frac{\partial w_0(x)}{\partial x} - \frac{\partial u_0(x)}{\partial x}\frac{\partial v_0(x)}{\partial x}\right)\right. \\
&\left. - \frac{M_{y1}+M_{y2}}{L}\left(\theta(x)\frac{\partial v_0(x)}{\partial x} + \frac{\partial u_0(x)}{\partial x}\frac{\partial w_0(x)}{\partial x}\right)\right] dx \\
&+ \frac{L}{2}\sum_{i=1}^{n} H_i\left[EI_{z\theta i}\left(\frac{\partial^2 v_0(x_i)}{\partial x^2}\right)^2 + EI_{y\theta i}\left(\frac{\partial^2 w_0(x_i)}{\partial x^2}\right)^2\right] \\
&+ \frac{L}{4}\sum_{i=1}^{n} H_i P\left[2y_{s\theta i}\frac{\partial w_0(x_i)}{\partial x} - 2z_{s\theta i}\frac{\partial v_0(x_i)}{\partial x}\right]\frac{\partial \theta(x_i)}{\partial x} \\
&+ \frac{L}{2}\sum_{i=1}^{n} H_i M_b \beta_{\omega\theta i}\left(\frac{\partial \theta(x)}{\partial x}\right)^2 \\
&+ \frac{L}{2}\sum_{i=1}^{n} H_i M_{y1}\frac{L-x_i}{L}\frac{\partial \theta(x_i)}{\partial x}\left[\frac{1}{2}\beta_{y\theta i}\frac{\partial \theta(x_i)}{\partial x}\right] \\
&- \frac{L}{2}\sum_{i=1}^{n} H_i M_{y2}\frac{x_i}{L}\frac{\partial \theta(x_i)}{\partial x}\left[\frac{1}{2}\beta_{y\theta i}\frac{\partial \theta(x_i)}{\partial x}\right] \\
&+ \frac{L}{2}\sum_{i=1}^{n} H_i M_{z1}\frac{L-x_i}{L}\frac{\partial \theta(x_i)}{\partial x}\left[\frac{1}{2}\beta_{z\theta i}\frac{\partial \theta(x_i)}{\partial x}\right] \\
&- \frac{L}{2}\sum_{i=1}^{n} H_i M_{z2}\frac{x_i}{L}\frac{\partial \theta(x_i)}{\partial x}\left[\frac{1}{2}\beta_{z\theta i}\frac{\partial \theta(x_i)}{\partial x}\right]
\end{aligned}
\tag{13}
$$

in which, H_i is the weight factor of the i^{th} Gaussian point located at a distance x_i from the element starting point, see Figure 5; and n is the number of Gaussian points assumed as 5 in the current study.

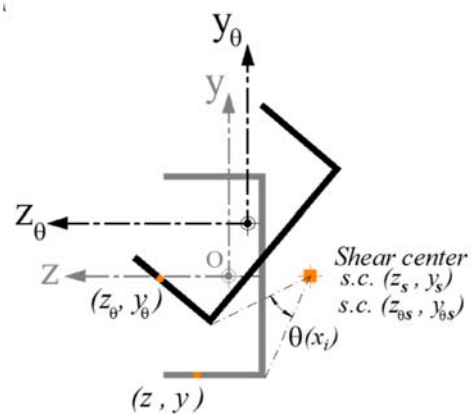

Figure 6. Illustrations of the section rotation at a general Gaussian point

3.4 Tangent Stiffness Matrix

As a result of the above and by taking the second variation of the total potential energy function (equation 2), the element stiffness matrix can be formulated as;

$$\delta^2\Pi = [k_E]\{\Delta u\} - \{\Delta f\} = 0 \tag{14}$$

where $[k_E]$ is the local element stiffness matrix accounting for the linear and geometric stiffness matrices, $[k_L]$ and $[k_g]$, respectively, and is given as;

$$[K_E] = [\mathrm{T}]([k_L] \odot [\xi_L] + [k_G] + [k_U] \odot [\xi_U])[\mathrm{T}]^T \tag{15}$$

where, $\odot$ represents the Hadamard product; $[k_U]$ is the additional geometric matrix by Liu et al. (2018) to account for the misalignment of the shear center and the cross-section centroid; $[\xi_L]$ and $[\xi_U]$ are the modification matrices which are calculated and given by L. Chen et al. (2020); and $[T]$ is, as mentioned earlier, the transformation matrix for the element deformations to reference the centroidal axis which is given as,

$$
[T] = \begin{bmatrix}
1 & 0 & 0 & 0 & 0 & 0 & 0 & 0 & 0 & 0 & 0 & 0 & 0 \\
0 & 1 & 0 & 0 & 0 & 0 & 0 & 0 & 0 & 0 & 0 & 0 & 0 \\
0 & 0 & 1 & 0 & 0 & 0 & 0 & 0 & 0 & 0 & 0 & 0 & 0 \\
0 & -z_{s\theta 1} & y_{s\theta 1} & 1 & 0 & 0 & 0 & 0 & 0 & 0 & 0 & 0 & 0 \\
0 & 0 & 0 & 0 & 1 & 0 & 0 & 0 & 0 & 0 & 0 & 0 & 0 \\
0 & 0 & 0 & 0 & 0 & 1 & 0 & 0 & 0 & 0 & 0 & 0 & 0 \\
0 & 0 & 0 & 0 & 0 & 0 & 1 & 0 & 0 & 0 & 0 & 0 & 0 \\
0 & 0 & 0 & 0 & 0 & 0 & 0 & 1 & 0 & 0 & 0 & 0 & 0 \\
0 & 0 & 0 & 0 & 0 & 0 & 0 & 0 & 1 & 0 & 0 & 0 & 0 \\
0 & 0 & 0 & 0 & 0 & 0 & 0 & 0 & 0 & 1 & 0 & 0 & 0 \\
0 & 0 & 0 & 0 & 0 & 0 & 0 & 0 & -z_{s\theta 2} & y_{s\theta 2} & 1 & 0 & 0 \\
0 & 0 & 0 & 0 & 0 & 0 & 0 & 0 & 0 & 0 & 0 & 1 & 0 \\
0 & 0 & 0 & 0 & 0 & 0 & 0 & 0 & 0 & 0 & 0 & 0 & 1
\end{bmatrix}
\tag{16}
$$

4. Numerical Procedure

After generating the element stiffness matrix, the global stiffness matrix needs to be assembled; while the element's local axes are transformed to a single global system utilizing the transformation matrix $[L]$ per McGuire et al. (2000). The numerical procedure where the element stiffness matrix $[k_E]$ is updated at each load increment is shown in Figure 7. Accordingly, the global stiffness matrix $[k_T]$ for a number of elements (NELEM) constructing the whole model is expressed as,

$$[k_T] = \sum_{i=1}^{NELEM} [L]\,([\Gamma][k_E]_i[\Gamma]^T)\,[L]^T \qquad (17)$$

Afterwards, the node displacements are calculated at each load increment; and hence, the node coordinates are updated so that the new member lengths are determined. As a sequel, the total element's end forces are updated. The summary of the incremental-iterative procedure is presented in Figure 7. Herein, the Updated-Lagrangian method is used for tracking the large-deflection behaviour while it is refined so that the element deformations are taken into account in addition to the nodal displacements and element forces. Hence, accurate predictions of the total member deformations are established employing the proposed Gaussian line-elements (Figure 3).

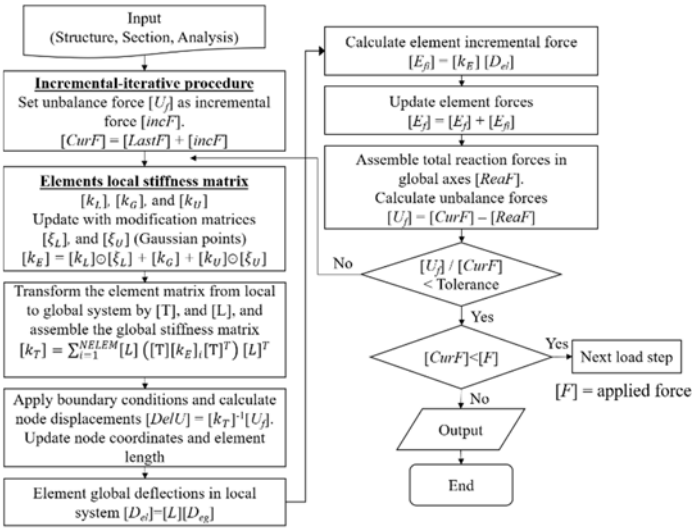

Figure 7. Flow chart for the numerical procedure of the proposed G.B.C. element

5. Verification Examples

In this section, verification examples to prove the accuracy and efficiency of the proposed Gauss line-element are presented. Cantilever beams with two cross-sections; (1) monosymmetric I-section, and (2) channel section, as shown in Figure 8, are studied. The member length is 6.0 m, and the material constants are Young's modulus E (= 210 Gpa), and Poisson's ratio ν (= 0.3). Incremental-iterative scheme shown in Figure 7 is adopted with 40 load steps. A concentrated bending moment (M) is applied at the cantilever end while a torsion moment (T) is imposed with twisting levels ($T/M = 0.1, 0.2, 0.3, 0.4$). The results from the conventional warping line element by Liu et al. (2018) and those resulted from the proposed Gaussian line element are given for comparisons. Herein, the results obtained from the warping element with 32 elements to model the beam represent the benchmark results. The applied bending moment versus lateral displacements are plotted in Figure 9, for monosymmetric I-section, and Figure 10 for channel section. As a sequel, the maximum displacements from different line elements for the cantilever with monosymmetric I-section are summarized in Table 1.

Based on the analysis results in Figure 9, Figure 10, and Table 1, it is clearly seen that the results obtained from the proposed Gaussian line-element, utilizing 8 or 4 elements to model the beam, agree well with the warping element using 32 elements. It is worthy of noting that even though the applied torsion on the beam is relatively small, the mono-symmetry of the sections makes the differences between results from 8 or 4 warping elements, and 32 warping elements are sizable. The results from Gaussian line-elements are, however, in line with those from 32 warping elements under both small and large twisting. Further, it can be noticed that the results of 4 Gaussian line-elements are more accurate than those of 8 warping elements. As a result of the above, it can be concluded that the proposed element can precisely and efficiently be implemented for simulating the asymmetrical section members utilizing fewer elements, thereby improving the numerical efficiency dramatically.

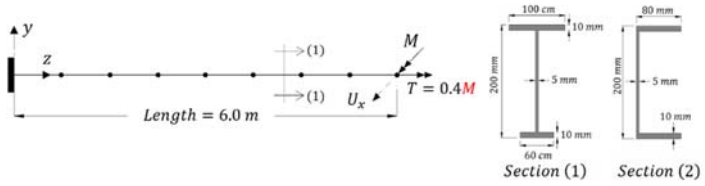

Figure 8. Cantilever beam with monosymmetric-I and channel sections

6. Conclusion

Nonsymmetrical section members usually experience complex behavior due to the non-coincidence of the shear-center and the cross-section centroid. Moreover, the twisting deformations of such members make the inclined angle between the element's local axes, and the cross-section axes vary along the member length. Hence, utilizing four or fewer conventional warping elements to model a structural member under sever torsion leads to significant errors when

predicting its global behaviour. In this paper, a new Gaussian line-element, based on the Gauss quadrature method to integrate the total potential energy function and accounting for the twisting deformations along the element length, is provided. A number of 5 Gaussian points is placed along the element length, whereas the twisting angle (θ) is calculated and included in the element formulation. From verification examples, it can be clearly seen that the proposed Gaussian line-element can precisely predict the large-deflection behavior of asymmetrical section members implementing fewer elements to simulate the member, thereby improving the numerical efficiency significantly. Finally, the Updated-Lagrangian method is refined so that a consideration of the element deformation along the element is included.

Table 1. Results summary for a member with monosymmetric I-section

T/M*	Maximum displacement (mm)								
	32 Elements	4 Elements				8 Elements			
	Warping element	Warping element		GBC		Warping element		GBC	
	(Benchmark)		**Diff.**		**Diff.**		**Diff.**		**Diff.**
0.1	138.3	153.57	**11.04%**	147.41	**6.59%**	144.55	**4.52%**	142.96	**3.37%**
0.2	128.38	158.14	**23.18%**	133.34	**3.86%**	138.76	**8.09%**	133.09	**3.67%**
0.3	69.05	102.06	**47.81%**	71.84	**4.04%**	80.15	**16.08%**	69.82	**1.12%**
0.4	32.68	55.43	**69.61%**	34.83	**6.58%**	40.33	**23.41%**	33.66	**3.00%**

*Note: *T* is the trosion moment, and M is the applied bending moment.

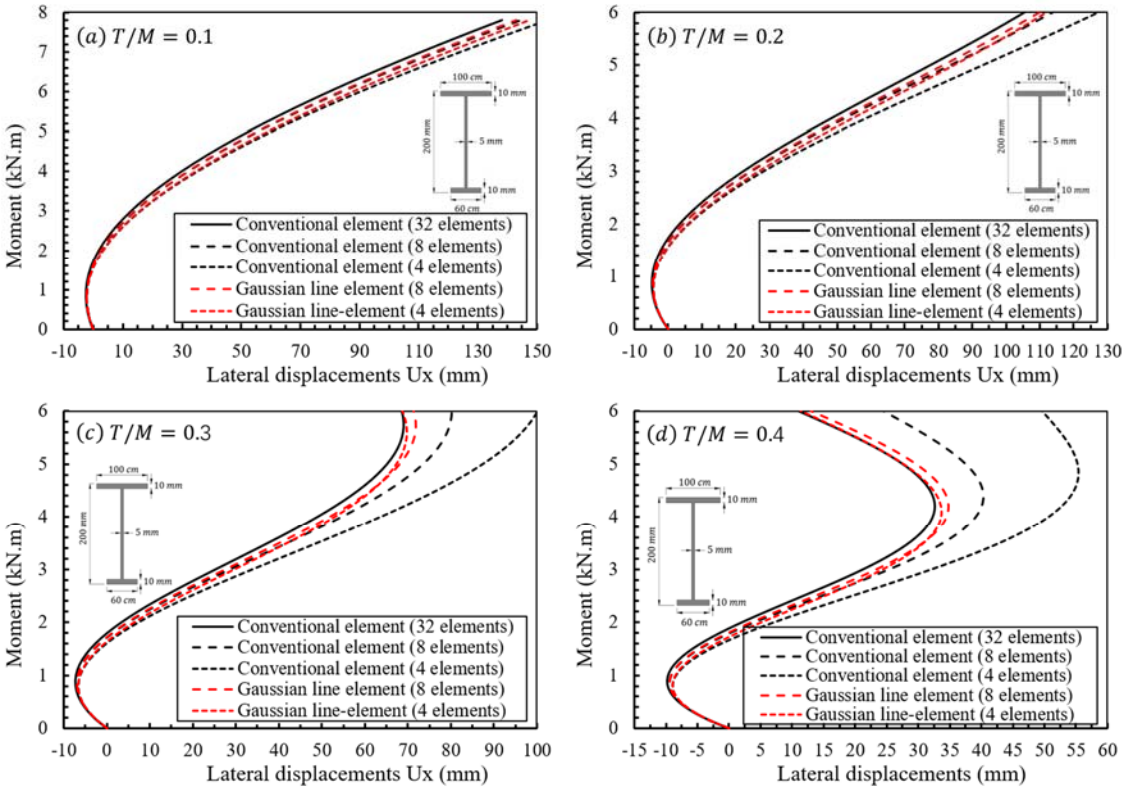

Figure 9. Applied moment versus lateral displacements for the cantilever with monosymmetric I-section

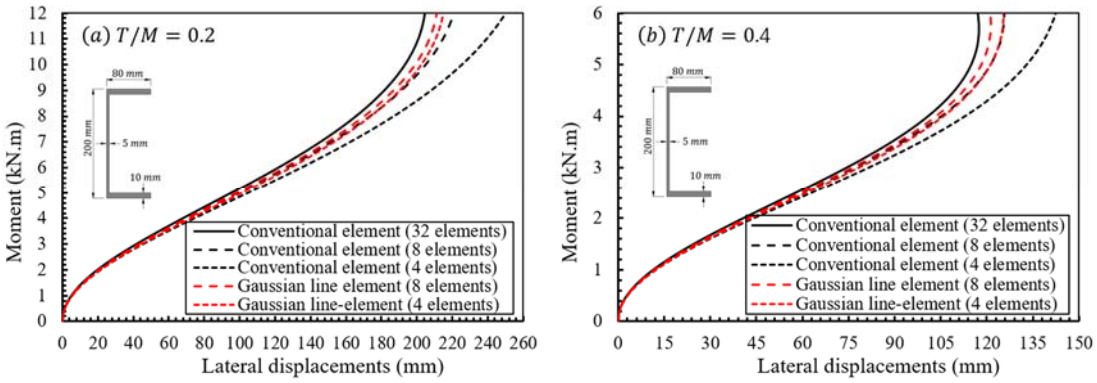

Figure 10. Applied moment versus lateral displacements for the cantilever with channel section

7. ACKNOWLEDGMENTS

The first author would like to express his gratitude to Johns Hopkins University for providing an excellent research environment for conducting this research. The last author is grateful for the financial support from the Hong Kong Polytechnic University. The authors want to sincerely acknowledge Professor Ronald D. Ziemian for his guidance and helping on conducting this research.

References

Abdelrahman, A. H. A., Du, Z. L., Liu, Y. P., & Chan, S. L. (2019). Stability design of single angle member using effective stress-strain method. *Structures, 20*, 298-308.

Abdelrahman, A. H. A., Liu, Y. P., Liu, S. W., & Chan, S. L. (2020). Simulation of thin-walled members with arbitrary-shaped cross-sections for static and dynamic analyses. *International Journal of Structural Stability and Dynamics (IJSSD)*. doi:doi: 10.1142/S021945542050128X

Ádány, S., & Schafer, B. W. (2014). Generalized constrained finite strip method for thin-walled members with arbitrary cross-section: primary modes. *Thin-Walled Structures, 84*, 150-169.

AISC (American Institute of Steel Construction). (2016). AISC specification. Specification for structural steel buildings. American Institute of Steel Construction. In. Chicago (IL).

Bai, R., Gao, W. L., Liu, S. W., & Chan, S. L. (2020). Innovative high-order beam-column element for geometrically nonlinear analysis with one-element-per-member modelling method. *Structures, 24*, 542-552.

Bai, R., Liu, S. W., Chan, S. L., & Yu, F. (2019). Flexural Buckling Strength of Tapered-I-Section Steel Columns Based on ANSI/AISC-360-16. *International Journal of Structural Stability and Dynamics, 19*(11), 1950134. doi:10.1142/s0219455419501347

Bathe, Klaus-Jurgen, & Bolourchi, S. (1979). Large displacement analysis of three-dimensional beam structures. *International journal for numerical methods in engineering, 14*(7), 961-986.

Bathe, K. J. (2007). Finite element method. *Wiley encyclopedia of computer science engineering*, 1-12.

Bian, G. (2017). *Modeling cold-formed steel members and systems.* Johns Hopkins University,

Bian, G., Peterman, K. D., Torabian, S., & Schafer, B. W. (2016). Torsion of cold-formed steel lipped channels dominated by warping response. *Thin-Walled Structures, 98*, 565-577.

British Standards Institution. (2005). British Standards Institution (BSI), BS EN 1993-1-1: 2005 Eurocode 3: Design of steel Structures Part 1-1: General Rules and Rules for Building,. In. London: BSI.

Chan, S. L., & Cho, S. H. (2008). Second-order analysis and design of angle trusses Part I: Elastic analysis and design. *Engineering Structures, 30*(3), 616-625.

Chan, S. L., & Gu, J. X. (2000). Exact tangent stiffness for imperfect beam-column members. *Journal of structural engineering, ASCE, 126*(9), 1094-1102.

Chan, S. L., & Kitipornchai, S. (1987). Geometric nonlinear analysis of asymmetric thin-walled beam-columns. *Engineering Structures, 9*(4), 243-254. doi:https://doi.org/10.1016/0141-0296(87)90023-X

Chan, S. L., & Zhou, Z. H. (1994). Pointwise equilibrating polynomial element for nonlinear analysis of frames. *Journal of structural engineering, ASCE, 120*(6), 1703-1717.

Chen, L., Abdelrahman, A. H. A., Liu, S. W., Ziemian, R. D., & Chan, S. L. (2020). Gaussian Line-Element Formulations for Large-Deflection Analysis of Beam-Column with Nonsymmetrical Sections. *AISC Journal of Structural Engineering (Under review).*

Chen, W. F., & Lui, E. M. (1987). Effects of joint flexibility on the behavior of steel frames. *Computers & Structures, 26*(5), 719-732.

Cho, S. H., & Chan, S. L. (2008). Second-order analysis and design of angle trusses, Part II: Plastic analysis and design. *Engineering Structures, 30*(3), 626-631.

Connor, J., Logcher, R. D., & Chan, S. C. (1968). Nonlinear analysis of elastic framed structures. *Journal of the Structural Division, ASCE, 94*(6), 1525-1548.

Dinis, P. B., Camotim, D., & Silvestre, N. (2006). GBT formulation to analyze the buckling behaviour of thin-walled members with arbitrarily 'branched'open cross-sections. *Thin-Walled Structures, 44*(1), 20-38.

Du, Z. L., Liu, Y. P., & Chan, S. L. (2017). A second-order flexibility-based beam-column element with member imperfection. *Engineering Structures, 143*, 410-426.

Fong, M., & Chan, S. L. (2012). advanced analysis of steel–concrete composite beam-columns by refined plastic hinge method. *International Journal of Structural Stability and Dynamics, 12*(06), 1250046. doi:10.1142/s0219455412500460

Gao, W. L., Abdelrahman, A. H. A., Liu, S. W., & Ziemian, R. D. (2020). Second-order dynamic time-history analysis of beam-columns with nonsymmetrical thin-walled steel sections. *Thin-Walled Structures (Under review)*.

Gonçalves, R., Ritto-Corrêa, M., & Camotim, D. (2010). A new approach to the calculation of cross-section deformation modes in the framework of generalized beam theory. *J Computational Mechanics, 46*(5), 759-781.

Hancock, G. j., & Rasmussen, K. (2016). *Formulation and implementation of general thin-walled open-section beam-column elements in opensees*. Retrieved from

Hussain, A., Liu, Y. P., & Chan, S. L. (2018). Finite element modeling and design of single angle member under bi-axial bending. *Structures, 16*, 373-389.

Iu, C. K., & Bradford, M. A. (2010). Second-order elastic finite element analysis of steel structures using a single element per member. *Engineering Structures, 32*(9), 2606-2616.

Izzuddin, B., & Smith, D. L. (1996). Large-displacement analysis of elastoplastic thin-walled frames. I: formulation and implementation. *Journal of structural engineering, ASCE, 122*(8), 905-914.

Kim, M. Y., Chang, S. P., & Kim, S. B. (1996). Spatial stability analysis of thin-walled space frames. *International journal for numerical methods in engineering, 39*(3), 499-525.

Liew, J. R., Chen, H., & Shanmugam, N. (1999). *Stability functions for second-order inelastic analysis of space frames.* Paper presented at the Light-Weight Steel and Aluminium Structures, Proc., 4th Int. Conf. on Steel and Aluminium Structures.

Liu, S. W., Gao, W. L., & Ziemian, R. D. (2019). Improved line-element formulations for the stability analysis of arbitrarily-shaped open-section beam-columns. *Thin-Walled Structures, 144*, 106290.

Liu, S. W., Liu, Y. P., & Chan, S. L. (2014a). Direct analysis by an arbitrarily-located-plastic-hinge element—Part 1: Planar analysis. *Journal of Constructional Steel Research, 103*, 303-315.

Liu, S. W., Liu, Y. P., & Chan, S. L. (2014b). Direct analysis by an arbitrarily-located-plastic-hinge element—part 2: spatial analysis. *Journal of Constructional Steel Research, 103*, 316-326.

Liu, S. W., Ziemian, R. D., Chen, L., & Chan, S. L. (2018). Bifurcation and large-deflection analyses of thin-walled beam-columns with non-symmetric open-sections. *Thin-Walled Structures, 132*, 287-301.

Martins, A. D., Camotim, D., & Dinis, P. B. (2018a). Distortional-global interaction in lipped channel and zed-section beams: Strength, relevance and DSM design. *Thin-Walled Structures, 129*, 289-308.

Martins, A. D., Camotim, D., Gonçalves, R., & Dinis, P. B. (2018b). On the mechanics of local-distortional interaction in thin-walled lipped channel beams. *Thin-Walled Structures, 128*, 108-125.

Mazzoni, S., McKenna, F., Scott, M. H., & Fenves, G. L. (2006). The open system for earthquake engineering simulation (OpenSEES), user command-language manual.

McGuire, W., Gallagher, R., & Ziemian, R. D. (2000). *Matrix Structural Analysis, John Wiley and Sons*.

Neuenhofer, A., & Filippou, F. C. (1997). Evaluation of nonlinear frame finite-element models. *Journal of structural engineering, ASCE, 123*(7), 958-966.

Neuenhofer, A., & Filippou, F. C. (1998). Geometrically nonlinear flexibility-based frame finite element. *Journal of structural engineering, ASCE, 124*(6), 704-711.

Oran, C. (1973). Tangent stiffness in plane frames. *Journal of the Structural Division, ASCE, 99*(6), 973-985.

Schafer, B. W. (2002). Local, distortional, and Euler buckling of thin-walled columns. *Journal of structural engineering, ASCE, 128*(3), 289-299.

Schafer, B. W., & Peköz, T. (1998). Computational modeling of cold-formed steel: characterizing geometric imperfections and residual stresses. *Journal of Constructional Steel Research, 47*(3), 193-210.

Shakourzadeh, H., Guo, Y. Q., & Batoz, J. L. (1995). A torsion bending element for thin-walled beams with open and closed cross sections. *J Computers & Structures, 55*(6), 1045-1054.

So, A. K. W., & Chan, S. L. (1991). Buckling and geometrically nonlinear analysis of frames using one element/member. *Journal of Constructional Steel Research, 20*(4), 271-289.

Souza, R. d. (2000). *Force-based finite element for large displacement inelastic analysis of frames.* (Ph.D.), University Of California, Berkeley,

Spacone, E., Ciampi, V., & Filippou, F. C. (1996). Mixed formulation of nonlinear beam finite element. *Computers & Structures, 58*(1), 71-83. doi:https://doi.org/10.1016/0045-7949(95)00103-N

Tang, Y. Q., Liu, Y. P., & Chan, S. L. (2018). A co-rotational framework for quadrilateral shell elements based on the pure deformational method. *Advanced Steel Construction (IJASC), 14*(1), 90-114.

Teh, L. H. (2001). Cubic beam elements in practical analysis and design of steel frames. *Engineering Structures, 23*(10), 1243-1255.

Wood, R. D., & Zienkiewicz, O. C. (1977). Geometrically nonlinear finite element analysis of beams, frames, arches and axisymmetric shells. *Computers & Structures, 7*(6), 725-735.

Yu, C., & Schafer, B. W. (2007). Simulation of cold-formed steel beams in local and distortional buckling with applications to the direct strength method. *Journal of Constructional Steel Research, 63*(5), 581-590.

Ziemian, R. D., McGuire, W., & Liu, S. W. (2019). MASTAN2 v5. In.

Zienkiewicz, O. C., Taylor, R. L., & Zhu, J. Z. (2005). *The finite element method: its basis and fundamentals* (6th Edition ed.): Elsevier.